Experiments on a Metal Hydride based Hydrogen Compressor

F. Laurencelle[*], Z. Dehouche[1], F. Morin, J. Goyette

Hydrogen Research Institute, Université du Québec à Trois-Rivières, 3351 Boul. Des Forges, Trois-Rivières, CP 500, G9A 5H7 Canada

Abstract

A three-stage metal hydride based hydrogen compressor prototype was built. It has been initially constructed for a hydrogen production facility using a low-pressure alkaline electrolyser. The compression system has been designed to transfer heat recovered from the electrolyser in the hydride beds to allow hydrogen desorption flow. The three-stage compressor achieves a compression ratio of 20:1 atm. It performs a thermal cycling of three AB_5 hydrides between 20 and 80°C. Its flow rate, for 25 g of each hydride bed, reaches about 20 L (NTP) of hydrogen per hour. The prototype is now operational. Some improvements in the heat transfer management system are also carried out before proceeding to the interconnection with the electrolyser and to the extent that the hydrogen produced satisfies the high purity requirement of the hydrides used in the compressor.

Keywords: **Metal hydrides, Hydrogen, Compression, Electrolysis, Thermal cycling**

[*] Corresponding author. *E-mail address:* francois.laurencelle@uqtr.ca (F. Laurencelle).
[1] Current address: School of Engineering and Design, Brunel University, Uxbridge, Middlesex UB8 3PH, UK

1. Introduction

The hydrogen compression using a thermal sorption process is known since more than 40 years. It has been used successfully for hydrogen liquefaction in Joule-Thompson cycles for space projects [1]. The premium advantage of this technology is the absence of moving parts (low vibration, low noise and low maintenance costs) [2-4]. It also produces high purity compressed hydrogen. However, its energetic efficiency and capital cost are not yet competitive over the diaphragm compressor.

To get the full advantage of this technology, one should design an application where secondary heat is available to supply the thermal sorption compressor. We have addressed the case of a decentralised hydrogen facility, *e.g.* a fuelling station, where hydrogen would be produced by electrolysis. Since electrolysis is nearly 65% efficient, its waste heat could be recycled through the compression operation, which is required to store the hydrogen [5].

We have manufactured a metal hydride based hydrogen compressor that could pressurize a part of the hydrogen produced by a *Stuart Energy systems* 5 kW electrolyser. The latter generates 1 m^3 of hydrogen per hour at atmospheric pressure and operates at 75-80°C with a water loop cooling system. We assume that sufficient purification of the gas can be performed without previous compression and that a large amount of heat can be

recovered within the electrolyser's cooling system (up to 150 kJ per mol of H_2 produced). The interconnection project is described in much detail in our previous publications [5-6].

2. Design of the compressor

Our first prototype compressor (figure 1) is an autonomous device that does not require a specific hydrogen or heat supply. A commercial gas bottle provides high purity hydrogen at a pressure of ~1 atm while two thermal control baths, regulated at ~20°C and ~80°C respectively, assume the temperature control by circulating either cold or hot water through the cells containing each of the three hydride reactors. Atmospheric evacuation and vacuum pumping are connected next to the hydrogen inlet port of the system.

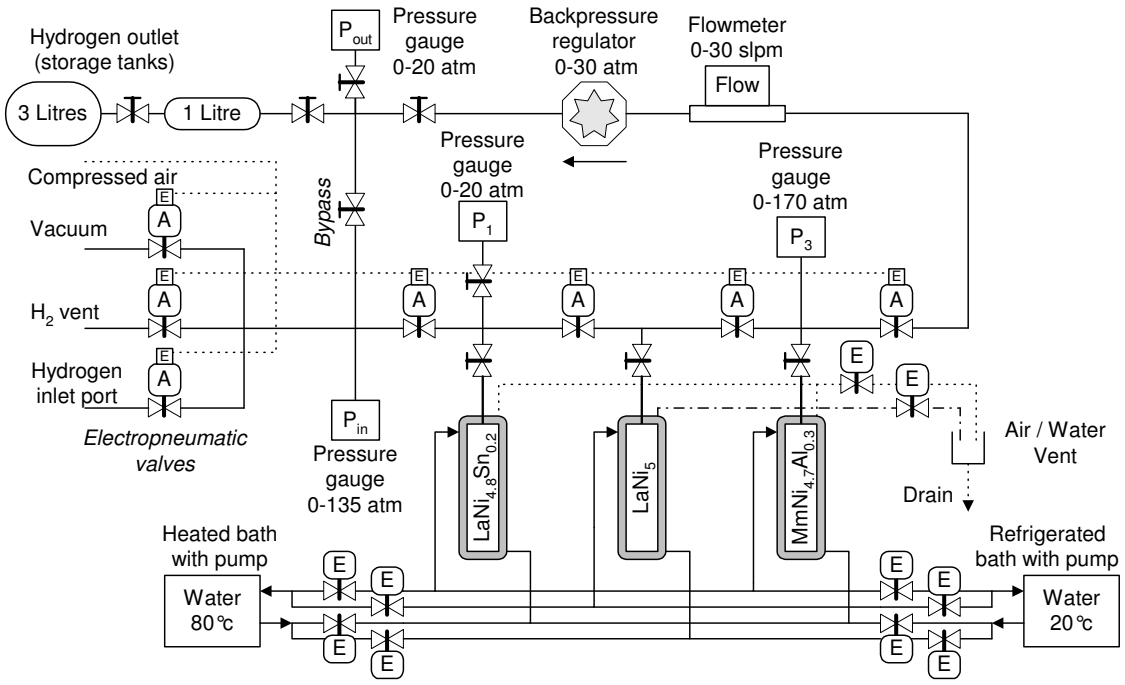

Figure 1. Schema of the compression system.

The hydrogen pressure increases through a series of three hydride reactors either cooled or heated. The hydrogen valves between the reactors are opened alternately to allow the hydrogen to move from a hot desorbing reactor to the cold absorbing reactor of the next stage. Finally, the compressed hydrogen is stored in a tank (1.05 or 4.20 litres). The bypass valve is opened for purging the whole system or when the outlet tank is used as buffer for special measurements, *e.g.* pressure-composition-temperature (PCT). A backpressure regulator (BPR) has been installed after the third hydride reactor to regulate the outlet flow rate, which is measured directly by a 30 sLpm mass flow meter. Four pressure transducers have been installed, respectively at the hydrogen inlet and outlet ports and at the first and third hydride reactors.

The hydrogen piping is built from ¼ inch stainless pipes and the water circulates into 3/8 brass pipes and flexible hoses. Electro-pneumatic diaphragm valves are used for

hydrogen, and solenoid valves, for water. The system is designed for an outlet hydrogen pressure of 20 atm but it is proofed for 50 atm. The 8 ml cylindrical hydride reactors are made of aluminium (diameter = 15.8 mm, height = 80 mm). Aluminium foams are press-fitted inside them, providing enhanced reaction bed heat transfer rate of ~8 W/mK [7]. These reactors are connected to the rest of the system through stainless VCR ½ connectors into which stainless filters of 2 µm pore size have been inserted. Each reactor can store 25 g of any AB_5 type hydride. Three polycarbonate tubes enclose the hydride reactors. They are tightened between plates and sealed with rubber gaskets. The water circulates inside these containers either to cool or heat the reactors.

The system is automated using a custom electronic interface, a USB data acquisition card and the software *LabView 7* from *National Instruments*. The experimental sequences are programmed through batch files and the readings are saved in text files with time stamps.

Alloys selection

Each reactor of the compressor is filled with an AB_5 type hydride, respectively $LaNi_{4.8}Sn_{0.2}$, $LaNi_5$ and $MmNi_{4.7}Al_{0.3}$. When put in contact with hydrogen, they absorb the gas if the gas pressure is beyond a plateau pressure P_{pl} specific to each alloy and that is a function of the temperature (van't Hoff rule):

$$(1) \qquad \ln P_{pl} = \frac{\Delta H}{\Re T} - \frac{\Delta S}{\Re},$$

where ΔH and ΔS are respectively the reaction enthalpy and entropy variations, $\Re$ is the gas constant (8.314 J/molK) and T is the absolute temperature in K. Similarly, the alloys release (desorb) the hydrogen when the gas pressure drops below that plateau pressure. The plateaux are characterized by step-by-step hydrogen loading and unloading measurements called PCTs where each point corresponds to a stabilized pressure-composition-temperature point. Since the measured plateau pressure is greater during hydrogen loading than unloading, we define the hysteresis η that compares the absorption and desorption plateau pressures P_{abs} and P_{des}.

$$(2) \quad \eta = \ln \frac{P_{abs}}{P_{des}},$$

The same way, the plateaux rise a little with the increasing hydrogen concentration in the hydride phase, so we define the plateau slope:

$$(3) \quad \sigma = \frac{d\left(\ln P\right)}{dC_H},$$

where C_H is the equilibrium hydrogen concentration for given pressure and temperature.

The PCT curves of the selected alloys are shown in figure 2 and their properties are given in table 1.

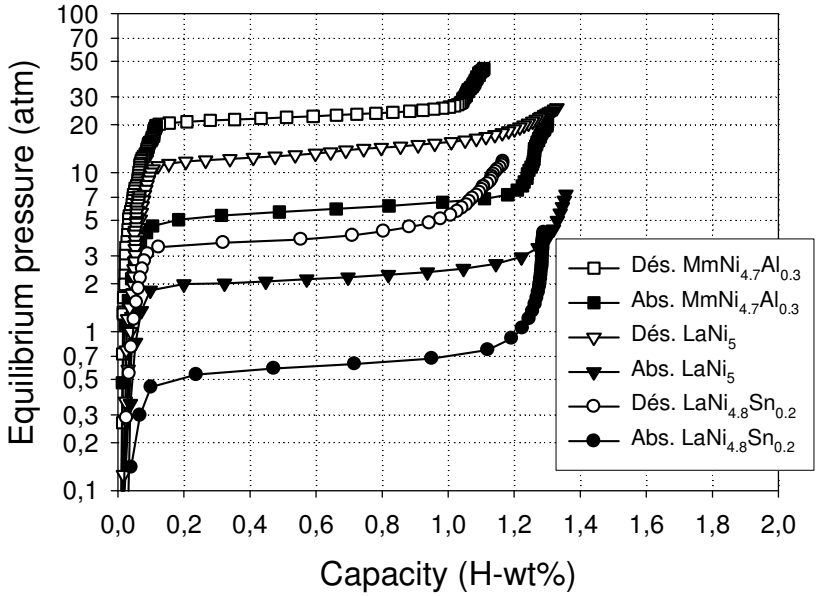

Figure 2. PCT curves of the hydrides used in the compressor.

Table 1. PCT properties of the hydrides used in the compressor.

	T (°C) ±2	P_{abs} (atm) ±0.02	P_{des} (atm) ±0.02	C_{max} (H-pds%) ±0.02	C_{pl} (H-pds%) ±0.03	*Hyst.* η (–) ±0.03	*Slope* σ (–) ±0.03	ΔH (kJ/mol) ΔS (kJ/molK) ±1%
$LaNi_{4.8}Sn_{0.2}$	22	0.61	0.46	1.28	1.23	0.27	0.33	-31.3
…	80	4.65	3.80	1.13	1.07	0.20	0.26	-0.101
$LaNi_5$	21	2.20	1.56	1.35	1.29	0.34	0.24	-30.7
…	80	16.69	13.63	1.30	1.21	0.30	0.19	-0.110
$MmNi_{4.7}Al_{0.3}$	23	5.91	3.49	1.21	1.17	0.53	0.29	-27.8
…	80	35.19	22.61	1.11	0.97	0.44	0.23	-0.107

The hydrogen concentration are C_{max} (at saturation) and C_{pl} (plateau width); the pressures P_{abs}, P_{des}, the hysteresis η and plateau slope σ were evaluated at the centre of the plateaux.

The first alloy, $LaNi_{4.8}Sn_{0.2}$ forms one of the most corrosion-resistant hydride for gas-solid reaction as demonstrated in several papers [7-9]. That feature is very important for the first hydride stage because it faces all the residual contamination from the input flow. The second alloy, $LaNi_5$, has a great sorption capacity and it exhibits very flat plateaux in PCT, but it has also a little tendency to disproportionate after thousands of cycles [9]. Eventually, one might expect to replace it by a lanthanum-rich mischmetal compound with tin (Sn) or aluminium (Al) substitution to improve its cycling life. The third alloy, $MmNi_{4.7}Al_{0.3}$ is a cerium-based mischmetal compound where Mm = $La_{0.321}Ce_{0.505}Pr_{0.046}Nd_{0.129}$. The aluminium substitution has also a suitable effect on the

corrosion resistance of AB_5 hydrides [10]. This alloys has a high sorption capacity compared to many alloys with higher levels of substitution that reach the same plateau pressures. In table 1, we observe that the sorption capacities of these alloys are about 1.3 H-wt% while their plateau are more narrow, about 1 H-wt%. The plateau pressures of these three hydrides, at both 20 and 80°C, have been adjusted carefully in order to obtain convenient pressure gradients and hydrogen transfer rates between consecutive compressor stages.

The $LaNi_{4.8}Sn_{0.2}$ and $MmNi_{4.7}Al_{0.3}$ samples were prepared from pure metal pieces: La (99.9%) from *Aldrich*, Ni, Sn and Al (99.95%) from *Alfa Aesar* and Mm (99%) from *Treibascher Auermet*. These elements were weighed under argon atmosphere and melted in an electric arc furnace to produce 30 g of each alloy. The samples were annealed at 950°C in vacuumed quartz tubes during 48 hours. On the other hand, the $LaNi_5$ (99.9%) has been bought from *Alfa Aesar* and used as is. Then, the three samples were kept under high hydrogen pressure (up to 45 atm) for about 12 hours and several cycles were carried out to complete their activation; after which their absorption and desorption kinetics were very fast. Figure 3 shows an example of kinetic measurements for the first hydride ($LaNi_{4.8}Sn_{0.2}$), in *P-T* conditions similar to compressor operation. Both the absorption and desorption reactions are completed within 5 minutes. That sample absorbs 1.24 H-wt% and desorbs 1.14 H-wt%. Similar behaviours have been observed with the two other samples.

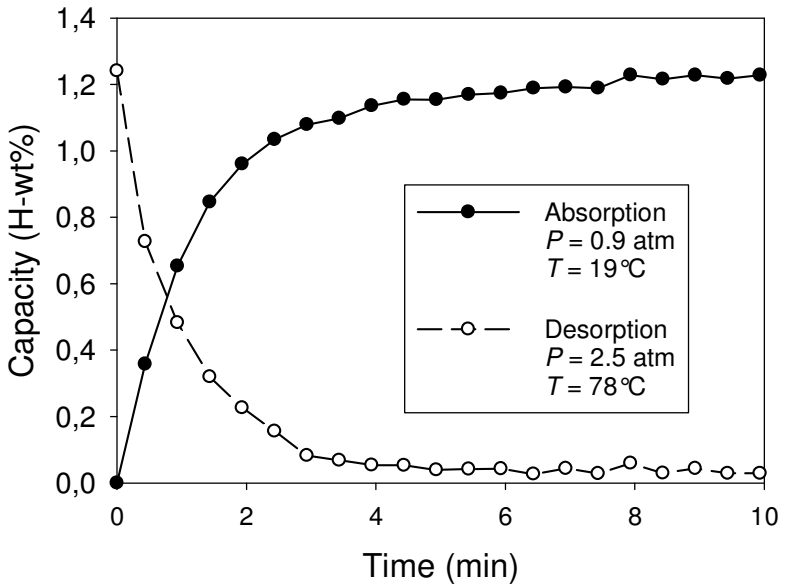

Figure 3. Kinetic profiles of the hydrides used in the compressor.

Compression experiments

Eleven hydrogen compression experiments were carried out to evaluate the compressor stability under various operating conditions. A summary of these experiments is given in table 2.

Table 2. Compression experiments

Experiment	1	2	3	4[a]	5	6	7	8	9	10	11[b]
Cycle length (min)	20.5	7.9	8.5	10.5	21.0	15.5	20.7	20.4	20.5	20.7	20.7
P_{in} (atm)	1.4	1.3	0.9	1.0	1.3	1.0	1.1	1.1	1.0	1.3	1.1
T_{abs} (°C)	17	20	22	17	16	18	17	13	24	15	22
T_{des} (°C)	82	79	80	78	82	82	83	82	86	75	87
BPR setting (atm)	0	0	0	0	0	22.3	20.2	20.3	20.3	21.6	21.3
Number of cycles	10	13	16	14	9	12	8	7	8	9	27
C_{eff} (H-wt%)	0.94	0.72	0.48	0.54	1.01	0.67	0.90	0.94	0.82	0.52	0.92
C_{eff} (L/cycle)	2.76	2.09	1.41	1.58	2.97	1.96	2.63	2.74	2.40	1.54	2.69
Avg. flow (L/h)	8.1	15.9	10.0	9.0	8.5	7.6	7.6	8.0	7.0	4.5	7.8

[a] Beginning of experiment 4, since it was continued up to 43 cycles and 38 atm.
[b] In experiment 11, the outlet volume was 4.20 L instead of 1.05 L.

a) Operation regimes

Our first 5 experiments were carried out while letting the backpressure regulator completely open. This way, the desorption pressure of the third hydride ($MmNi_{4.7}Al_{0.3}$) followed that of the outlet tank, which increased by steps corresponding to each cycle. In experiment 4 (figure 4), two operation regimes have been observed. During the first 16 cycles, the outlet pressure increased stepwise up to about 25 atm while the absorption pressure of the same hydride stayed near 10 atm and the effective capacity (C_{eff}) was about 0.54 H-wt%. Beyond this threshold, the desorption of that hydride was limited by the too high outlet pressure (upper than its PCT plateau). Then it could be cycled only in the right side of its plateau. Consequently, its absorption pressure also increased and the effective capacity decreased progressively to 0.09 H-wt% in the subsequent cycles.

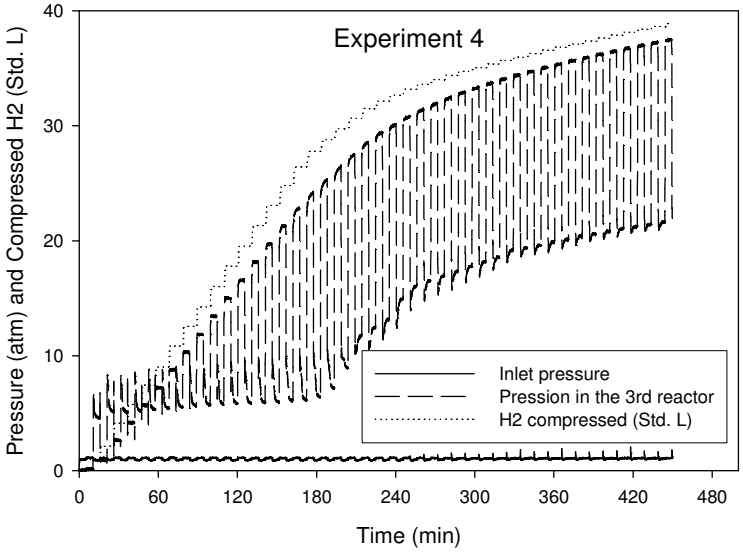

Figure 4. Pressure and hydrogen compressed profiles when exceeding the normal pressure range.

b) Backpressure regulator

The backpressure regulator (BPR) controls the desorption pressure of the last hydride regardless of the hydrogen pressure in the outlet tank. Experiments 1 and 7 were managed in similar conditions except for the use of the BPR. In experiment 1 (figure 5), not using the BPR, the peak flow measured in the first cycle was 21.0 sLpm and it decreased in further cycles. On the other hand, in experiment 7 (figure 6), the peak flow was the same at each cycle, 3.3 sLpm, due to the BPR. During that experiment, the cyclic behaviour stayed very regular until the pressure in the outlet tank of 1.05 L surpassed the BPR set point of 20.2 atm in the 8th cycle. With both methods, it took 8 cycles to fill the reservoir to 20 atm with similar effective capacities about 0.9 H-wt%. Therefore the BPR enables very stable cycling conditions with negligible effect on the average hydrogen flow.

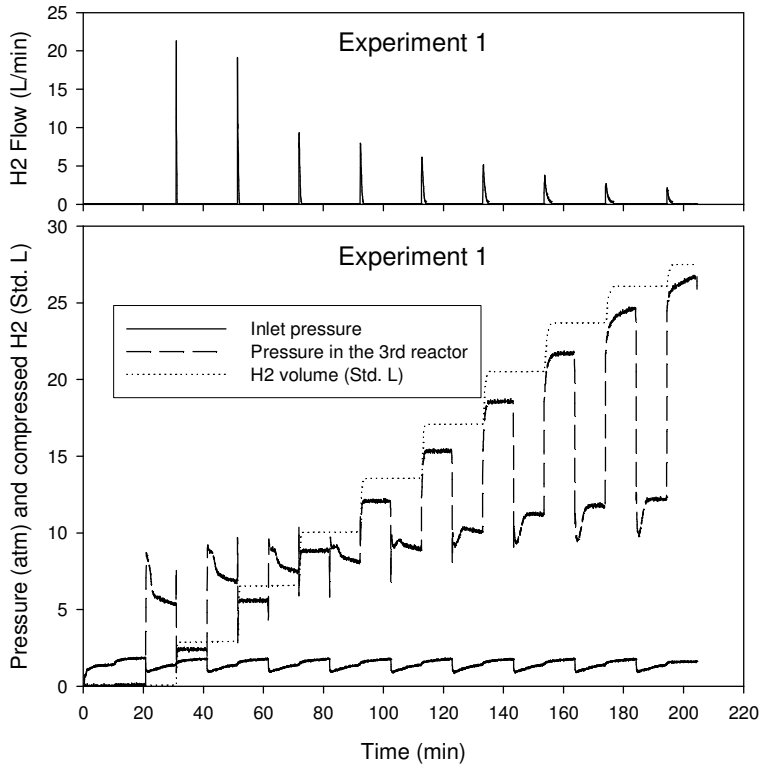

Figure 5. Flow, pressure and hydrogen compressed without outlet pressure regulation.

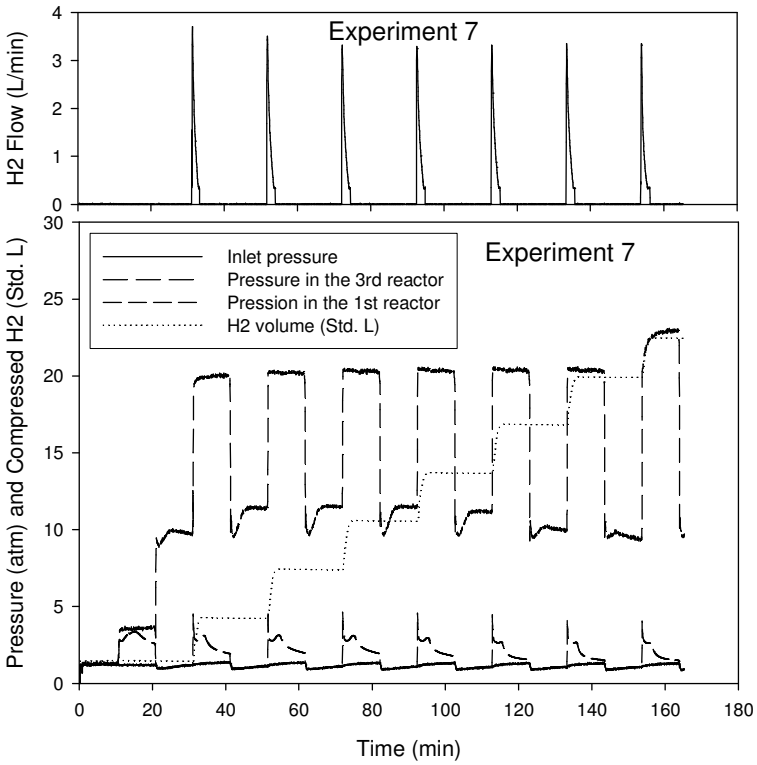

Figure 6. Flow, pressure and hydrogen compressed after setting the BPR to 20 atm.

c) Exchange pressure levels

The compressor works properly since the gap between the plateaux of a desorbing hydride and the following absorbing one is large enough to allow reasonably fast kinetics. Consequently, the exchange pressures between the consecutive stages must be found between these plateau pressures. The sensor P1 collects this information for desorption of reactor 1 and absorption in reactor 2. Similarly, the sensor P3 measures the exchange pressure for desorption of reactor 2 towards reactor 3. Typical measurements of all the sorption pressures and the corresponding temperature profiles are displayed in figure 7 and 8 for experiment 11. In table 3, we compare these exchange pressures to the corresponding plateau pressures, measured at the end of the half cycles. The large pressure gradients between consecutive stages encourage the hydrogen transfer. The exchange pressure at the end of the absorption in $LaNi_5$ is very close to its plateau because that hydride has the largest storage capacity. On the other hand, during the desorption of $LaNi_5$ and the absorption of $MmNi_{4.7}Al_{0.3}$, the pressure stabilizes at an intermediate value between their plateaux.

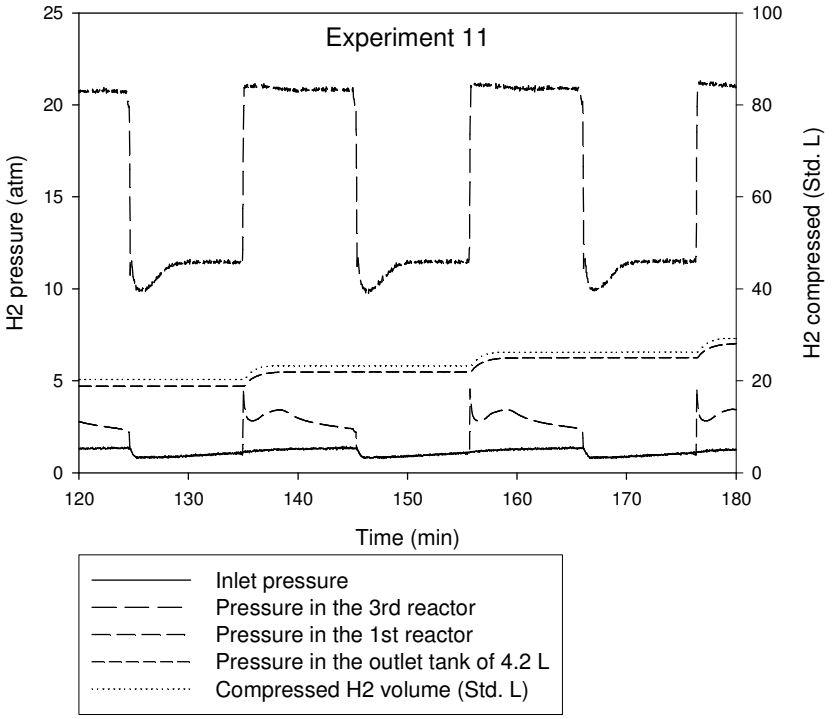

Figure 7. Enlarged view of the pressure and compressed hydrogen profiles during experiment 11.

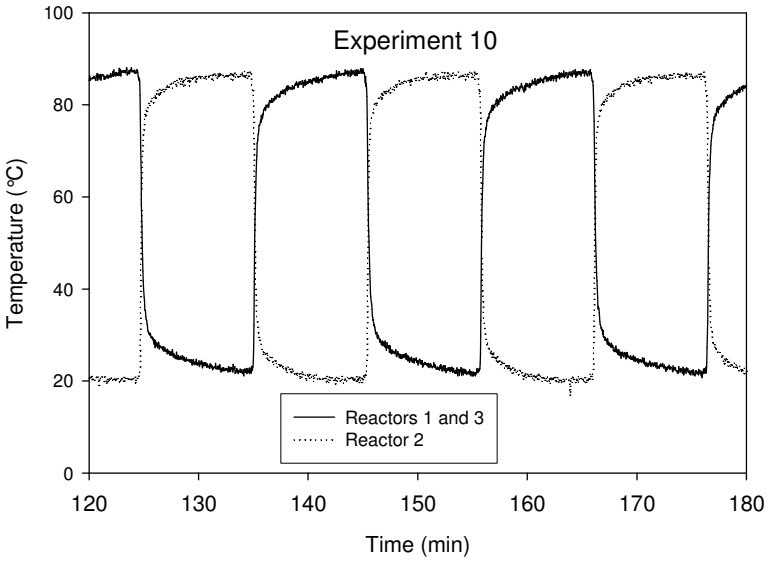

Figure 8. Enlarge view of the temperature profiles of experiment 11.

Table 3. Stabilisation pressures and plateau pressures during experiment 11.

Hydrogen transfer	Desorption plateau[a] P_{des} (atm)	Exchange pressure (atm)	Absorption plateau[a] P_{abs} (atm)
Inlet line	Regulated inlet		$LaNi_{4.8}Sn_{0.2}$

to reactor 1	hydrogen pressure	1.1	0.5 (0.7)
Reactor 1 to reactor 2	$LaNi_{4.8}Sn_{0.2}$ 5.4 (4.3)	2.2	$LaNi_5$ 2.1 (2.7)
Rreactor 2 to reactor 3	$LaNi_5$ 19.6 (15.4)	11.3	$MmNi_{4.7}Al_{0.3}$ 4.7 (7.0)
Reactor 3 to outlet line	$MmNi_{4.7}Al_{0.3}$ 36.1 (25.8)	21.3	Outlet pressure controlled by BPR

[a] The values in parenthesis account for the slope and the hysteresis while the other are computed from only the van't Hoff rule with ΔH and ΔS.

c) Tuning of the operating parameters

According to the fast kinetics of AB_5 hydrides (figure 3), the hydrogenation reactions were expected to reach equilibrium during the first five minutes of each half cycle. However, during our experimentations, the thermal control baths have been unable to drive such a fast thermal cycling. That is, the temperature gap between absorption and desorption temperatures declined when cycling at a faster rate than 20 min/cycle. A more effective heating/cooling system would allow increasing the hydrogen flow rate up to 20 L/hr by reducing the cycle duration.

The efficiency of the thermal compression is directly proportional to the amount of hydrogen compressed at each cycle. The effective capacity C_{eff} is given in table 2 for each experiment. We have intended to fit these results to a function of ln P_{in}, T_{abs} and T_{des} using a linear equation:

$$(4)\quad C_{eff} = k_{in} \ln P_{in} + k_{abs} T_{abs} + k_{des} T_{des} + k_{const.}$$

where the coefficients k are obtained by linear regression: P_{in} should be expressed in atm and T_{abs} and T_{des}, in Kelvin.

That regression gives the parameter values listed in table 3. The adjustment has a coefficient of determination R^2 = 0.95. Although the linearity in this relation is an empirical assumption, the capacities are predicted adequately, with only a 4% error, within the range of our experimentations (figure 9).

Table 4. Linear regression of the capacity over the conditions of the compression experiments (Coefficient of coordination $R^2 = 0.95$) .

Coefficient	Value	Std. dev.
k_{in}	0.623	±0.128
k_{abs}	-0.0254	±0.0061
k_{des}	0.0565	±0.0055
k_{const}	-11.94	±2.97

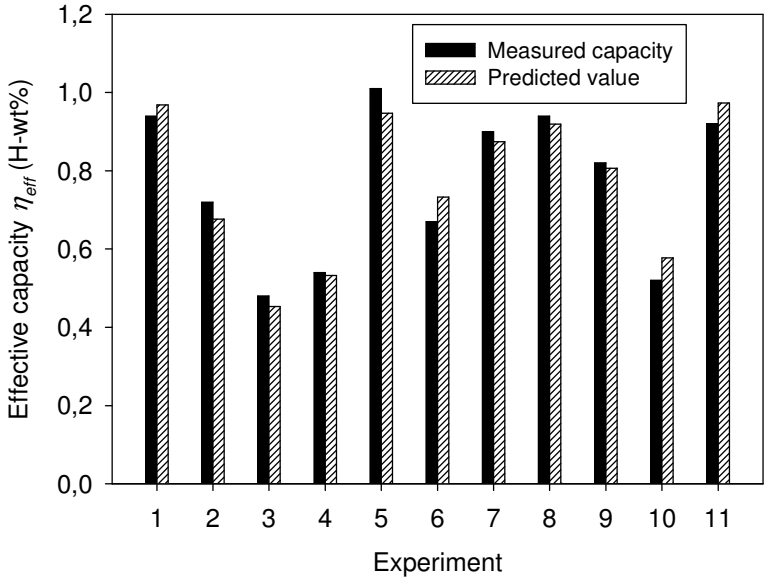

Figure 9. Predicted effective capacities vs. experimental values.

The coefficient k_{in} is expected to represent the contribution of the absorption kinetics of the first hydride. A common model [11-12] would express that reaction rate such as:

$$(5)\ \frac{dC_H}{dt} \propto k_{in}\left[\ln P_{in} - \ln P_{abs}^{1}\right],$$

where C_H is the concentration of hydrogen already stored in the sample (in H-wt%) and $\ln P_{abs}^{1}$ should be computed using the van't Hoff relation with the data of $LaNi_{4.8}Sn_{0.2}$ and the absorption temperature. Then, the coefficient $k_{abs} \approx -k_{in}\Delta H^{1}/\Re T_{abs}^{2}$ has the proper magnitude to stands for the second part ($k_{in}\ln P_{abs}^{1}$) of that kinetic dependence.

On the other hand, k_{des} is about 2.5 times greater than k_{abs} and it constitutes the main contribution of the all the other reactions. Its value is coherent with a hard to complete desorption process in one of the hydrides since the plateau shifting due to the temperature set points can influence the equilibrium concentration C_H. The last hydride's desorption during experiment 10 is an example of a hard desorption process. Indeed, one can find from equations 1 and 2 that:

$$(6)\ k_{des} \approx \frac{dC_H}{dT} = \frac{1}{\sigma}\cdot\frac{\Delta H}{\Re T_{des}^{2}}.$$

However, a thorough review of the hydride behaviour close to their plateaux would be suitable to explain more accurately the performance of multistage hydride compressors.

Referring to table 2, when the inlet pressure is about 1 atm or less (at experiments 3, 4 and 6), the capacity tends to decrease. In experiment 3, this behaviour is brought to the fore by a harmfully high absorption temperature of 22°C. Similarly, when the desorption temperature goes below 80°C (in experiments 2, 3, 4 and 10), the capacity also declines substantially. The case of experiment 9 is particular: the unfavourable absorption conditions have been compensated by a very favourable desorption temperature; so the capacity remained in the intermediate range. In that case, the hydrides have desorbed to their full capacity, then the left part of the plateau, which needs less pressure to be fulfilled with hydrogen, could have also participated to the cycling.

Discussion

After this prototype study, we have identified some research issues that should be addressed to achieve a more competitive performance with a hydride based hydrogen compressor. Firstly, it is essential to minimise the thermal storage capacity of the inert parts of the system that undergo thermal cycling, including the hydride reactor shell, the connecting nuts, a part of the tubing and a share of the heat transfer fluid. Secondly, a single stage design, where the hydride would be heated to a higher desorption temperature, would need less enthalpy energy. However, a more intensive thermal cycling regime could precipitate the degradation of the materials used, including the hydrides, since most AB_5 compounds are prone to disproportionate when heated over 100°C [13]. Few improvements to the process efficiency can be expected from modifications of the hydrides themselves. The viable hydrides for this application are AB_5, AB_2 or AB compounds, for which the enthalpy of the hydrogenation reaction is in the range of -20 to -35 kJ/mol, depending on their working pressure range. We have previously studied a set of $(Ti,Zr)(V,Mn)_{1.3\text{-}1.6}$ alloys to reach sorption capacities up to 2 H-wt%. However, these alloys were difficult to produce, their plateaux were bended and a part of their capacity was lost during the activation cycle, so they appeared less suitable than AB_5 for compression applications [14]. Due to the above-mentioned limitations, the energy efficiency of hydride compressors would never exceed 20-25%. On the other hand, scaling the compressor for a smaller quantity of hydride and compensate the flow rate with fast cycling could reduce the capital cost of the system. The performance of a smaller design would be conditioned by the swiftness of the temperature control in the hydride reactors. The flow rate is maximal at the beginning of each half-cycle reaction. One can over-size the heat transfer system to promptly stabilize the temperature in every hydride cell and shorten the cycle time. The interconnection of an electrolyser and a hydride compressor would become feasible after developing efficient low-pressure gas purification and drying apparatus to be installed between the two systems. New pressurized electrolysers would generate enough pressure to purify the hydrogen by filtering. The hydrogen could then be compressed to a convenient storage pressure, *e. g.* 200 atm, with a similar metal hydride compression system. However, the thermal energy recoverable from an electrolyser is still lean. It will allow a maximum compression ratio of 20:1, with a hydride-based compressor if we discard any additional energy input.

Conclusion

Safe and convenient hydrogen compression system are crucial for the introduction of hydrogen into energy markets. Metal hydrides hydrogen compressor technology is feasible but remains at the prototype development phase. It offers great potential for special applications niche due to some attractive characteristics: no moving parts, no vibration, no noise, safety, high purity, low maintenance. However, its capital cost and its efficiency need a breakthrough to compete with diaphragm compressors, still about two times more efficient. Moreover, some applications like electrolysis production where compression is a secondary process and where low-grade heat is available would benefit of its thermodynamic operating mode. The compressor we have developed has shown very reliable operation and reached our expectations in term of efficiency and compression flow performance. We are also developing innovative concepts of sorption vessels [16] for efficient thermal management, which can truly improve the hydrogen compressor performance. In particular the concept of micro-channel container. it is a micro-structured system that can pack a lot of power into a small space and dissipate effectively on small surfaces the heat of the sorption reactions.

Acknowledgements
The authors are grateful for the financial support of Natural Resources Canada (NRCan) and Ministère des Ressources Naturelles et de la Faune du Québec (MRNF). One of us (F.L.) also wants to thank Natural Sciences and Engineering Research Council of Canada (NSERC) for a grant.

References

1. R.C. Bowman Jr., Development of metal hydride beds for sorption cryocoolers in space applications, J. Alloys and Compounds 356-357 (2003) 789-793.

2. M. Golben, D.H. DaCosta, Advanced thermal hydrogen compression, In Proceedings of the 2001 U.S. DOE Hydrogen Program Review, Baltimore, MD: NREL/CP-570-30535.

3. Z. Feng, B. Deyou, J. Lijun, Z. Liang, Y. Xiaoyu, Z. Yiming, Metal hydride compressor and its application in cryogenic technology, J. Alloys and Compounds 231 (1995) 907-909.

4. E.P. Da Silva, Industrial prototype of a hydrogen compressor based on metallic hydride technology, Int. J. Hydrogen Energy 18,4 (1993) 307-311.

5. F. Laurencelle, Z. Dehouche, J. Goyette, T.K. Bose, Integrated electrolyser—metal hydride compression system, Int. J. Hydrogen Energy 31,6 (2006) 762-768.

6. Z. Dehouche, N. Grimard, F. Laurencelle, J. Goyette and T.K. Bose, Hydride alloys properties investigations for hydrogen sorption compressor, J. Alloys and Compounds 399,1-2 (2005) 224-236.

7. A. Rodríguez Sánchez, H.P. Klein, M. Groll, Int. J. Hydrogen Energy 28 (5) (2003) 515–527.

8. F. Laurencelle, Z. Dehouche, J. Goyette, Hydrogen sorption cycling performance of $LaNi_{4.8}Sn_{0.2}$, J. Alloys and Compounds 424,1-2 (2006) 266-271.

9. S.W. Lambert, D. Chandra, W.N. Cathey, F.E. Lynch, R.C. Bowman, Investigation of hydriding properties of $LaNi_{4.8}Sn_{0.2}$, $LaNi_{4.27}Sn_{0.24}$ and $La_{0.9}Gd_{0.1}Ni5$ after thermal cycling and aging, J. Alloys and Compounds 187,1 (1992) 113-135.

10. R.C. Bowman Jr., C.H. Luo, C.C. Ahn, C.K. Witham, B. Fultz, The effect of tin on the degradation of $LaNi_{5-y}Sn_y$ metal hydrides during thermal cycling, J. Alloys and Compounds 217,2 (1995) 185-192.

11. K. Nishimura, K. Sato, Y. Nakamura, C. Inazumi, K. Oguro, I. Uehara, S. Fujitani, I. Yonezu, Stability of $LaNi_{5-x}Al_x$ alloys (x=0~0.5 during hydriding and dehydriding cycling in hydrogen containing O_2 and H_2O, J. Alloys and Compounds 268,1-2 (1998) 207-210.

12. F. Askri, A. Jemni, S.B. Nasrallah, Study of two-dimensional and dynamic heat and mass transfer in a metal–hydrogen reactor, Int. J. Hydrogen Energy 28,5 (2003) 537-557.

13. U. Mayer, M. Groll, W. Supper, Heat and mass transfer in metal hydride reaction beds: Experimental and theoretical results, J. Less Common Metals 131,1-2 (1987) 235-244.

14. G. Friedlmeier, A. Manthey, M. Wanner, M. Groll, Cyclic stability of various application-relevant metal hydrides, J. Alloys and Compounds 231,1-2 (1995) 880-887.

15. Z. Dehouche, M. Savard, F. Laurencelle, J. Goyette, Ti–V–Mn based alloys for hydrogen compression system, J. Alloys and Compounds 400,1-2 (2005) 276-280.

16. Z. Dehouche, D. Lemay, J. Goyette, T.K. Bose, High Performance Gas Unit Storage Micro-Cell, Use Thereof in Portable Fuel Cells, in Zero Emission Vehicle and in Power Generation Plant, Patent pending (Application No. 2398195), Canadian Intellectual Property Office (2002). http://patents.ic.gc.ca/cipo/cpd/en/patent/2398195/summary.html.